

Real-time detection of PRT1-mediated ubiquitination via fluorescently labeled substrate probes

Augustin C. Mot,^{1,2,4} Erik Prell,^{3,5} Maria Klecker,^{1,2} Christin Naumann,^{1,2} Frederik Faden,^{1,2} Bernhard Westermann³ & Nico Dissmeyer^{1,2,*}

¹ Independent Junior Research Group on Protein Recognition and Degradation, Leibniz Institute of Plant Biochemistry (IPB), Weinberg 3, D-06120 Halle (Saale), Germany

² ScienceCampus Halle – Plant-based Bioeconomy, Betty-Heimann-Str. 3, D-06120 Halle (Saale), Germany

³ Department of Bioorganic Chemistry, Leibniz Institute of Plant Biochemistry (IPB), Weinberg 3, D-06120 Halle (Saale), Germany

⁴ present address: Faculty of Chemistry and Chemical Engineering, Babes-Bolyai University, 11 Arany Janos, Cluj-Napoca, Romania

⁵ present address: Max Planck Institute for Biophysical Chemistry, Am Fassberg 11, D-37077 Göttingen, Germany

*Correspondence should be addressed to N.D. (nico.dissmeyer@ipb-halle.de).

RUNNING TITLE

Live assays with fluorescent N-end rule substrates

KEY WORDS

activity profiling, labeling chemistry, protein labeling, fluorescence polarization, fluorescent dyes, fluorescent substrates, compound library screening, fluorophoric haloacetamides

ABSTRACT

The N-end rule pathway has emerged as a major system for controlling protein stability in medical, animal and plant sciences as well as agriculture. This included the discovery of novel functions and enzymes of the pathway. Ubiquitination mechanism and substrate specificity of *bona fide* N-end rule pathway E3 Ubiquitin ligases is still elusive. Taking the first discovered *bone fide* plant N-end rule E3 ligase PROTEOLYSIS1 (PRT1) as a model, we describe a novel tool to molecularly characterize polyubiquitinylation live, in real-time. We demonstrate that PRT1 is indeed an E3 ligase and gain mechanistic insights in PRT1 substrate preference and activation by monitoring live ubiquitination by using a fluorescent chemical probe coupled to artificial substrate reporters. Ubiquitination can then be measured by rapid in-gel fluorescence scanning in classical end-point assays as well as in real time by fluorescence polarization in standard microplate readers. Enzymatic activity, substrate specificity, reaction mechanisms and optimization can be easily investigated *ad hoc* in short time and with significantly reduced reagent consumption.

INTRODUCTION

The ON/OFF status of proteins within the cells' proteome, their general abundance and specific distribution throughout the compartments and therefore their functions and activities are precisely controlled by protein quality control (PQC) mechanisms to ensure proper life of any organism. Therefore, the biochemical analysis of the underlying mechanisms safeguarding proteostatic control is pivotal. It ranges from the molecular characterization of enzymes involved in PQC and their catalyzed reactions to enzyme-substrate to non-substrate protein-protein interactions. The so-called Ubiquitin (Ub) 26S proteasome system (UPS) is a master component of PQC with the central core units of non-catalytic Ub ligases (E3), the Ub-conjugating enzymes (E2), and the Ub-activating enzymes (E1).

To investigate an element conferring substrate specificity, we chose PROTEOLYSIS1 (PRT1) as a model E3 ligase, which is a *bona fide* single-subunit E3 with unknown substrate portfolio.¹⁻³ Its biological function remains elusive but it presumably represents a highly specific enzyme of the N-end rule pathway of targeted protein degradation, which is a part of the UPS. The N-end rule relates the half-life of a protein to its N-terminal amino acid⁴ and causes rapid proteolysis of proteins bearing so-called N-degrons, N-terminal sequences that lead to the degradation of the protein. N-degrons are created by endoproteolytic cleavage of protein precursors (pro-proteins) and represent the resulting neo-N-termini of the remaining C-terminal protein moiety, albeit not all freshly formed N-termini automatically present destabilizing residues (**Figure 1a**).

The N-end rule pathway is an emerging vibrant area of research and has a multitude of functions in all kingdoms.⁵⁻⁹ Identified substrates are mainly important regulatory pro-

teins and play key roles in animal and human health,¹⁰⁻¹⁴ plant stress response and agriculture.^{9, 15-20}

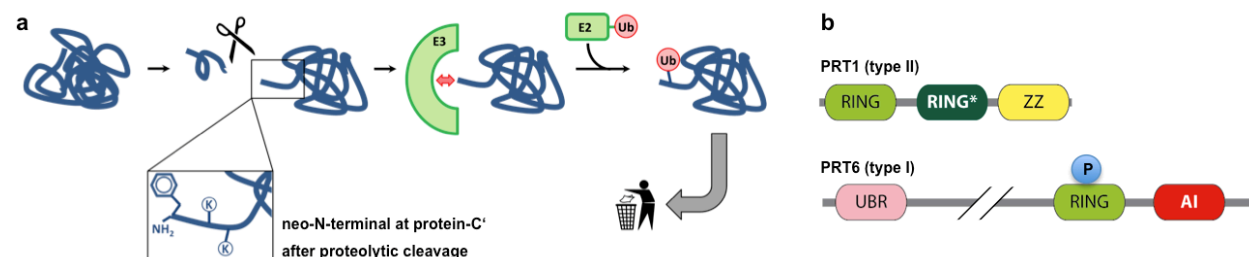


Figure 1. Generation of N-end rule substrates by proteolytic processing and predicted features of the two bone fide plant N-recognins. **a)** Substrates containing N-degrons can be generated from (pre-)pro-proteins as precursor sequences after proteolytic cleavage (indicated by the scissors). The N-degron shown here comprises a Phe residue as primary destabilizing residue at the protein-C' and internal lysines for polyubiquitination. These N-degrons can be recognized by N-end rule E3 Ub ligases (N-recognins) which in turn associate with Ub-conjugating enzymes (E2) carrying Ub which was previously activated by E1 enzymes. One possible result of ubiquitination is protein degradation and to date, in the context of the N-end rule, ubiquitination is assumed to lead to degradation in most of the cases. **b)** The two known *Arabidopsis* N-recognins were identified by their function (PRT1, 46 kDa) and by homology to the UBR-box from *S. cerevisiae* UBR1p (PRT6, 224 kDa). UBR: box binding type I substrates; RING*: composite domain containing RING and CCCH-type Zn fingers; ZZ: Zinc binding domain similar to RING; RING: protein-protein interaction domain for E2-E3 interaction; AI: predicted autoinhibitory domain (intramolecular interaction); P: phosphorylation site (PhosPhAt 4.0; phosphat.uni-hohenheim.de). b is modified from Tasaki et al., 2012.

In plants, functions of N-end rule enzymes are associated with central developmental processes including seed ripening and lipid breakdown, hormonal signaling of abscisic acid (ABA), gibberellin and ethylene, with seed dormancy and germination,²¹⁻²³ with leaf and shoot morphogenesis, flower induction, and apical dominance,²⁴ and the control of leaf senescence.²⁵ Then, the pathway was shown to be a sensor for reactive oxygen species (ROS) by mediating nitric oxide (NO) signaling and regulating stress response after hypoxia, e.g. after flooding and plant submergence.¹⁵⁻¹⁷ A novel plant-specific class of enzymes was associated with the pathway, i.e. plant cysteine oxidases (PCOs), highlighting plant-specific molecular circuits, enzyme classes and mechanisms.¹⁸ In the moss *Physcomitrella patens*, N-end rule mutants are defective in gametophytic development²⁶ and protein tar-

gets of N-end rule-mediated posttranslational modifications were discovered.²⁷ Also in barley, the pathway is connected with development and stress responses.¹⁹ Only very recently, a link between N-end rule function and plant-pathogen response and innate immunity was found,²⁰ shedding light on novel functions of the yet underexplored branch of targeted proteolysis. However, to date, the identity of plant N-end rule targets still remains obscure and clear evidences from biochemical data of *in vitro* and *in vivo* studies such as N-terminal sub-proteomics or enzymatic assays are still lacking.

A novel *in vivo* protein stabilization tool for genetic studies in developmental biology and biotechnological applications, the 'It-degron', works in plants and animals by directly switching the levels of functional proteins *in vivo*.²⁸ The method is based on conditional and specific PRT1-mediated proteolysis, the process studied in depth with the here-generated fluorescent substrate reporters.

N-degrons are by definition recognized and the corresponding protein ubiquitinated by specialized N-end rule E3 ligases, so-called *N-recognins*.^{5, 7, 8, 29} In plants, only two of these, namely PRT1 and PRT6, are associated with the N-end rule (**Figure 1b**). This is in contrast to the high number of proteolytically processed proteins which carry in their mature form N-terminal amino acids that could potentially enter the enzymatic N-end rule pathway cascade.³⁰ In the light of more than 800 putative proteases in the model plant *Arabidopsis thaliana*, it is likely that the N-end rule pathway plays an important role on the half-lives of these protein fragments in a proteome-wide manner. Examples are found in the METACASPASE9 degradome, i.e. that part of the proteome which is associated with degradation,³¹ or the N-degradome of *E. coli*³² with a possibly analogous overlap with endosymbiotic plant organelles.³³

PRT1, compared to the *Saccharomyces cerevisiae* N-recognin Ubr1 (225 kDa), is a relatively small protein (46 kDa) and totally unrelated to any known eukaryotic N-recognins but with functional similarities to prokaryotic homologs (**Figure 1b**). It is therefore perceived as a plant pioneer E3 ligase with both diversified mechanistics and function. Artificial substrate reporters with N-terminal phenylalanine were shown to be stabilized in *prt1* mutant cells.¹⁻³ However, until today, there are neither *in vivo* targets nor direct functions associated with PRT1, however, very recently, a potential role of PRT1 in plant innate immunity was flagged.²⁰

The spectrum of N-termini possibly recognized by plant N-end rule E3 ligases including PRT1 is not sufficiently explored. Only Phe-starting test substrates were found to be stabilized in a *prt1* mutant whereas initiation by Arg and Leu still caused degradation.^{2, 3, 34} However, PRT1 was shown to destabilize also Tyr- and Trp-starting reporter proteins in a heterologous system in *S. cerevisiae*.³ In the light of substrate identification, it is cardinal to determine PRT1 mechanistics in more detail because several posttranslationally processed proteins bearing Phe, Trp and Tyr at the neo-N-termini were found^{30, 31} and hence represent putative PRT1 targets altogether. Elucidating the substrate specificity of PRT1 will be an important step forward towards substrate identification and association of PRT1 and the N-end rule with a biological context.

We established a technique that allows real time measurements of ubiquitination using fluorescence scanning of SDS-PAGE gels and fluorescence polarization. We propose its use as a generic tool for mechanistic and enzymological characterization of E3 ligases as master components of the UPS directing substrate specificity. With a series of artificial test

substrates comprising various *bona fide* destabilizing N-end rule N-termini, substrate specificity was analyzed and revealed PRT1 preference for Phe as a representative of the bulky hydrophobic class of amino acids. The *in vitro* ubiquitination methods used so far are based on end-time methods where the reaction is stopped at a given time point and analyzed by SDS-PAGE followed by immunostaining with anti-Ub versus anti-target specific antibodies. This detection via western blot often gives rise to the characteristic hallmark of polyubiquitinated proteins, a "ubiquitination smear" or a more distinct "laddering" of the posttranslationally Ub-modified target proteins. All the information of what occurred during the time of reaction is unknown unless the assay is run at several different time points which drastically increases both experimental time and reagent consumption. Existing fluorescence polarization measurements are more frequently used to characterize enzyme-substrate or protein-protein interactions rather than enzyme activity and parameters affecting the performance of the ubiquitination reaction.³⁵⁻³⁷ To our knowledge, there are no protocols available to monitor substrate ubiquitination in a time-resolved and live manner.

We then established a corresponding method that monitors this very process live, in real time, using fluorescently labeled substrate proteins and fluorescence-based detection assays, namely fluorescence polarization. In addition, the protocol was coupled to fast and convenient scanning fluorescence in-gel detection. This type of assay can be easily adapted for high-throughput measurements of ubiquitination and probably also similar protein modification processes involving changes in substrate modification over time *in vitro*.

Here, we report a novel advanced approach to molecularly characterize E3 ligases, to measure and track polyubiquitination live and in a time-resolved manner. It has the po-

tential to lead to profound implications for our understanding of the interactions of E3 ligases with substrates and non-substrates and can impact ubiquitination research in general as our work suggests to be transferable to other E3 ligases and enzyme-substrate pairs. The method relies on rapid, easy and cheap protocols which are currently lacking for in-depth biochemical analysis of E3 ligases and is at the same time non-radioactive, sterically not interfering, and works with entire proteins in form of directly labeled substrates.

So far, only three reports mention work on PRT1 at all, i.e. the two first brief descriptions^{2, 3} and one highlighting the role of the N-end rule pathway, in particular a novel function for PRT1, in plant immunity.²⁰ However, to date, the community lacks proofs demonstrating that PRT1 and other E3 candidates are indeed involved in substrate protein ubiquitination. To date, ubiquitination activities of E3 ligase candidates from the plant N-end rule pathway were only speculated. Here, we demonstrate for the first time that PRT1 is indeed involved in polyubiquitination of substrate proteins depending on its N-terminal amino acid.

RESULTS AND DISCUSSION

PRT1 is an E3 ubiquitin ligase and prefers bulky N-termini

For the analysis of PRT1 E3 ligase function, i.e. recognition of N-end rule substrates, we used recombinant PRT1 together with generic substrate reagents with unprecedented detection features combining chemically synthesized fluorophores and recombinant ubiquitination acceptors which were used as live protein modification detectors. To describe N-terminal amino acid specificity of PRT1, the N-terminally variable protein parts of the reporters were engineered as N-terminal His8:MBP fusions comprising a recognition se-

quence of tobacco etch virus (TEV) protease at the junction to the subsequent generic substrate protein moiety (**Figure 2a, Supplementary Figure 1a**). Cleavage by TEV gave rise to small C-terminal fragments of the His8:MBP-substrate fusions of which the neo-N-terminal, i.e. the P1' residue of the TEV cleavage site, can be altered to all proteinogenic amino acids except proline.³⁸⁻⁴⁰ For a novel fluorescence-based approach, we covalently coupled a synthetic fluorescent probe (**Figure 2b**) to the artificial substrate protein. The resulting reagent serves as fluorescent protein Ub acceptor in N-end rule ubiquitination assays. The architecture of the reagent is as follows: after the cleavable His8:MBP tag, eK, a part of *E. coli* lacZ⁴ followed by a triple hemagglutinin epitope tag (3HA) for immunodetection and an *E. coli* flavodoxin (Flv) were combined. Flv was chosen as a highly soluble and stable protein. The junctions between His8:MBP and eK encode for the N-termini glycine (Gly, G), phenylalanine (Phe, F), arginine (Arg, R), and leucine (Leu, L) that get N-terminally exposed after TEV cleavage. The G/F/L/R-eK-Flv constructs contain a single cysteine (Cys101 of Flv) that allowed the labeling of the purified recombinant fusion protein with a novel thiol-reactive probe that comprises a iodoacetamide-polyethylene glycol (PEG) linker and the fluorogenic subunit of 4-nitro-2,1,3-benzoxadiazole (NBD; **Figure 2b**). We chose the latter due to its small size compared to other labeling reagents such as large fluorescein moieties and because it can be detected very specifically by both UV absorption and UV fluorescence with low background interferences.

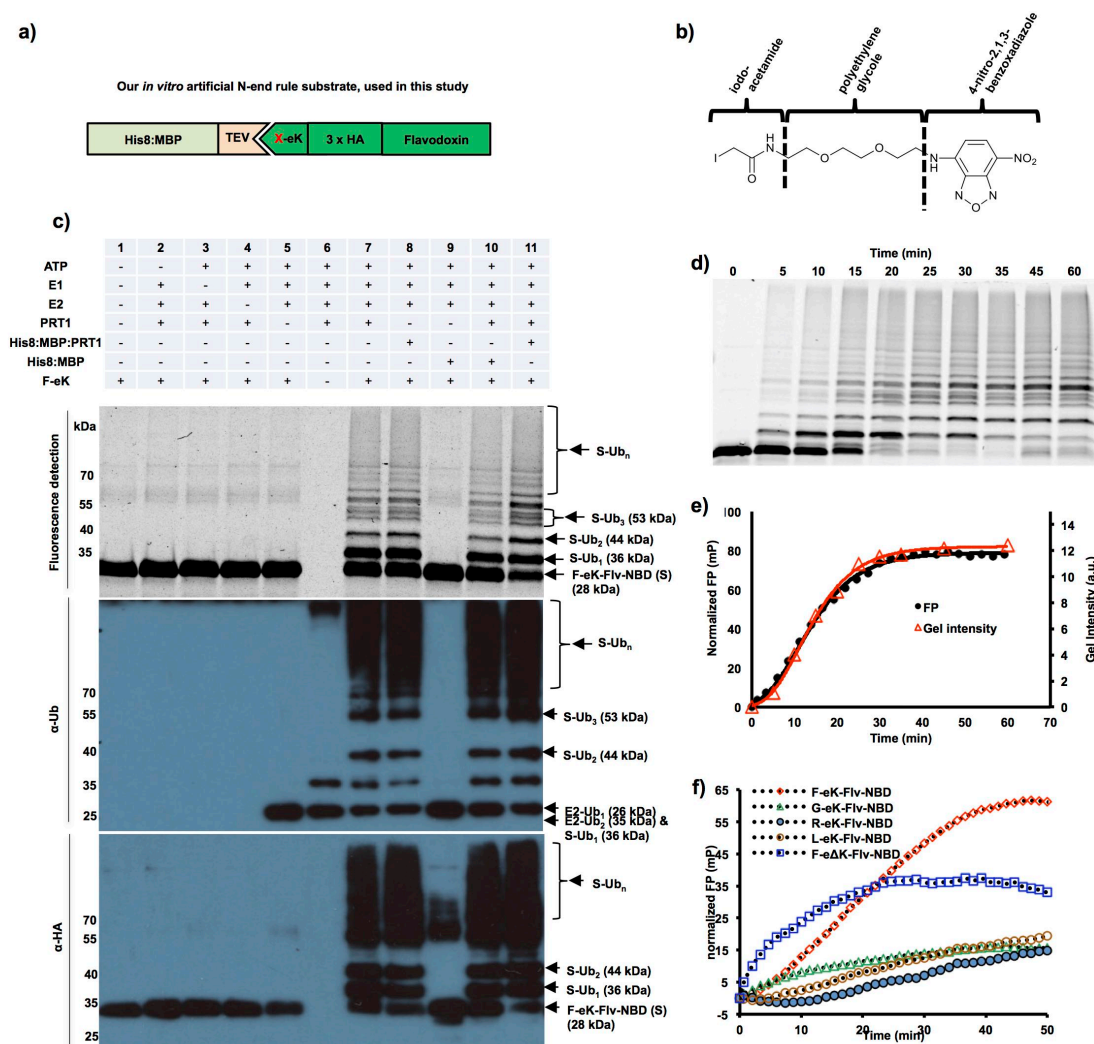


Figure 2. Fluorescent protein conjugates for monitoring *in vitro* substrate ubiquitination in real time. **a)** Design of recombinant fusion proteins used as N-end rule substrates. After TEV cleavage and removal of the His8:MBP affinity tag, the artificial substrate based on *E. coli* flavodoxin (Flv) is initiated with a neo-N-terminal, here Phe (F), Gly (G), Leu (L) or Arg (R). **b)** Skeletal formula of the synthesized thiol-reactive fluorescent compound. The substrate was covalently tagged with the reagent composed of iodoacetamide, polyethylene glycol (PEG) linker and 4-nitro-2,1,3-benzoxadiazole (NBD). The reactive iodine-containing group on the left couples to the thiol group of internal Cys residues of Flv. NBD serves as a fluorophore with excitation at 470 nm and emission at 520 nm. **c)** Detection via fluorescence and immunoblotting of the F-eK-Flv-NBD after *in vitro* ubiquitination. The labeled protein and its ubiquitinated variants were detected via fluorescence scanning directly from the SDS-PAGE gel followed by western blotting and immunodetection with anti-HA and anti-Ub antibodies. Lane 6 shows autoubiquitination of PRT1 at about 35 kDa and very high molecular weight. Cleaved PRT1 as well as His8:MBP-tagged PRT1 were used together with His:UBA1 (E1) and His:UBC8 (E2).⁴¹ **d and e)** Kinetic profiles of PRT1-mediated ubiquitination. F-eK-Flv-NBD ubiquitination was monitored by FP and in-gel fluorescence scanning. The S-shaped kinetic curve is observed in both in-gel fluorescence scanning detection and fluorescence polarization. **f)** N-terminal specificity evaluated by real-time ubiquitination detection. Fluorescently labelled R-eK-Flv, L-eK-Flv, G-eK-Flv, F-eΔK-Flv and F-eK-Flv were comparatively evaluated for their degree of ubiquitination by PRT1.

In an *in vitro* ubiquitination assay, we used recombinant UBC8 as a promiscuous E2 conjugating enzyme and UBA1 as E1 activating enzyme⁴¹ and show here for the first time E3 ligase activity of PRT1 depending on E1, E2 and ATP (**Figure 2c**). PRT1 discriminates a substrate by its N-terminal, aiding the transfer of Ub to the substrate and leading to polyubiquitination. Similar assays are evaluated based on immunochemical and colorimetric detection, incorporation of radioisotopes such as ¹²⁵I or ³²P, or fluorescently labeled native or recombinant Ub. After immunostaining with anti-Ub antibodies, usually, a typical smear of higher molecular weight compared to the target protein's size is observed or after probing with target-specific antibodies, a more or less distinct laddering, also of high molecular weight, becomes evident. These are the common signs for polyubiquitination and a clear laddering was also visualized by fluorescent scanning in our novel approach. We identified distinct subspecies via in-gel detection (**Figure 2c**). However, in this experimental setup, our assay can be evaluated immediately and gel-based after SDS-PAGE rendering protein transfer via western blotting plus the subsequent steps of blocking, immuno- and chemical detection obsolete.

A classical end-time point assay where the reaction was stopped at different reaction time points followed by SDS-PAGE and in-gel fluorescence detection revealed the kinetics of PRT1 activity using F-eK-Flv as substrate (**Figure 2d**). However, a real-time monitoring of the kinetic profile of the enzymatic reaction is only possible via fluorescence polarization (FP) in live detection measurements.

The protocol described in the following is rapid, non-radioactive, uses only a small fluorophore as covalent dye, works with full substrate proteins instead of only peptides, and can be read out live and in real-time. Moreover, the FP approach conveys superimpos-

able kinetic curves with data from classical end-time point assays, but faster, with higher resolution in time and using fewer reagents (**Figure 2e**). The kinetic profile is best-fitted with an S-shaped curve and a growth curve model of logistic type (Richards' equation) rather than exponentially as expected for simple kinetics. A possible explanation for the S-shaped kinetic curve and the presence of an initial lag phase in an increase of the affinity of PRT1 for the monoubiquitinated substrates compared to the non-ubiquitinated population. Preferences of E2s and E3s for mono- or polyubiquitinated substrates and their influence on ubiquitination velocity but also that initial ubiquitination greatly enhances the binding affinity of E3s to the substrate in subsequent reactions was shown previously.^{42, 43} Thus, the chain elongation (Ub-Ub isopeptide bond formation) is faster than the chain initiation which might represent the rate limiting-step of the reaction, rather than an E1-E2-controlled limiting-step, see below. Thus, the chain elongation and chain initiation steps appear to be distinct processes that have distinct molecular requisites in agreement with previous findings.^{44, 45} The lag phase is reduced if the rate is increased by higher concentration of PRT1.

It was previously suggested that PRT1 binds to N-degrons carrying bulky destabilizing residues.³ By changing the N-terminal residue of the X-eK-Flv-NBD substrate, it was possible to reveal that PRT1 indeed discriminates the substrates according to the N-terminal residue, as expected (**Figure 2f, Supplementary Figure 1b,c**). While the substrates carrying G-, R-, L-initiated N-termini showed poor ubiquitination, F-eK-Flv-NBD was heavily ubiquitinated. Additionally, the FP-based assay reveals that the kinetic profile of the ubiquitination is dependent on the position and availability of lysines as Ub acceptor sites as suggested as a characteristic of the N-degrons tested.⁴⁶ While the eK-based substrate

267 showed the kinetic curve discussed above, the control F-eΔK-Flv substrate with mutated
 268 lysines (expected site of ubiquitination, Lys15 and Lys17, both replaced by Arg) presented
 269 a faster initial rate of ubiquitination but levels of only half of the final FP value (**Figure 2f**).
 270 This is in good agreement with the in-gel fluorescence detection where lower degrees of
 271 ubiquitination of F-eΔK-Flv, reduced mono- and di- ubiquitination - but still clear polyubiq-
 272 uitination - were observed (**Supplementary Figure 1c**). This suggested that by lowering
 273 the overall number of available lysines in the substrate (two Lys less than in X-eK-Flv con-
 274 structs with 11 Lys in total) the overall ubiquitination was detectably reduced. However,
 275 this simple end-point assay could not unravel if this was due to altered velocity of chain
 276 initiation versus chain elongation. But the initiation per Lys residue was expected to be
 277 similar in eK- versus eΔK-Flv substrates but chain elongation could apparently start faster
 278 in F-eΔK-Flv. This demonstrates that the presences of E2 together with the particular sub-
 279 strate play key roles in the formation of the molecular assembly facilitating the ubiquitina-
 280 tion process. Already the intermolecular distance between the E3 ligase and the Ub accep-
 281 tor lysines of the substrate as well as the amino acid residues proximal to the acceptor ly-
 282 sines determine the progress of the reaction and ubiquitination specificity.⁴² Taking the
 283 slower initiation of polyubiquitination of F-eΔK-Flv into account, the availability of lysines
 284 at the N-terminus might interfere with the monoubiquitination of other, more distal lysines
 285 and the E3 could remain associated with substrates that are monoubiquitinated at the N-
 286 terminal.

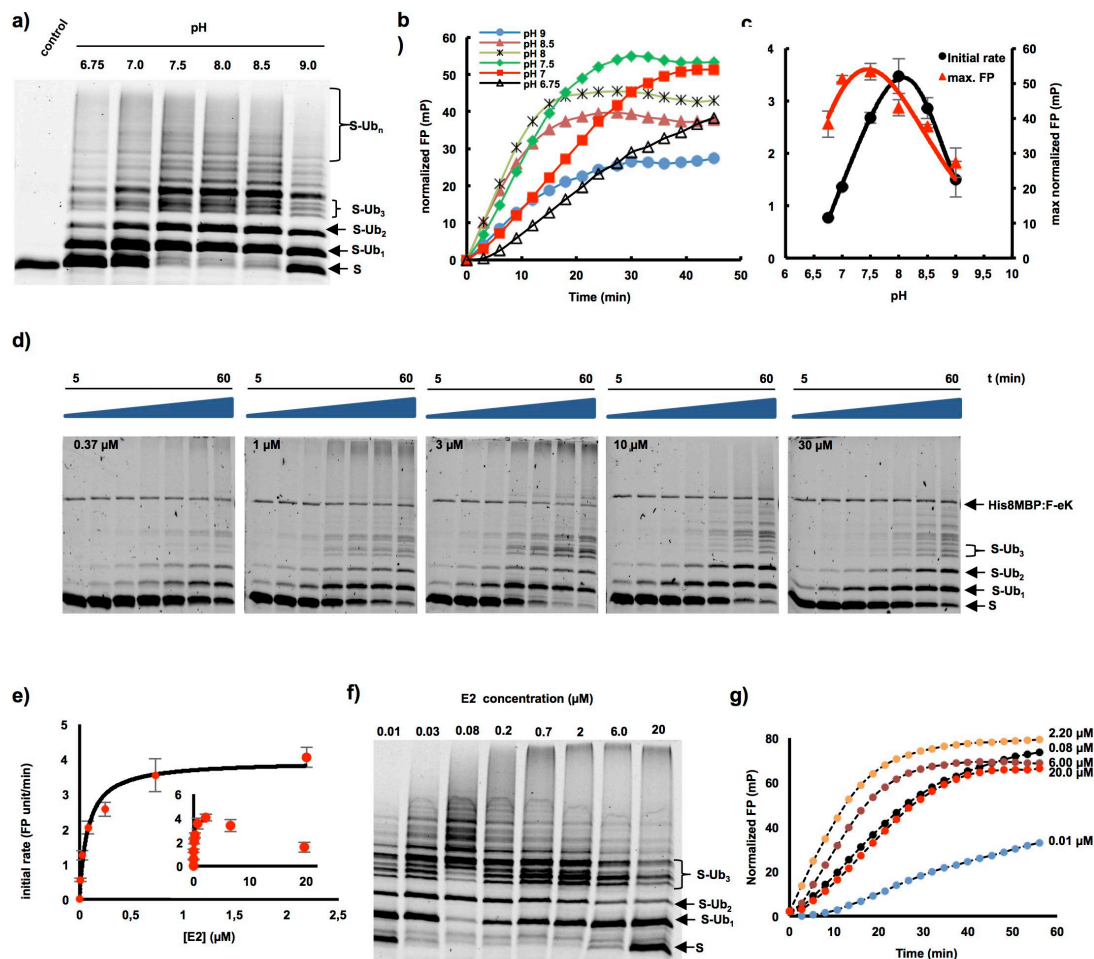


Figure 3. Applications of fluorescent protein conjugates for monitoring pH dependent ubiquitination and enzymatic parameters of PRT1 E3 ligase. a-c) pH dependent ubiquitination of the F-eK-Flv substrate. **a)** In-gel detection of F-eK-Flv ubiquitinated species after 1 h reaction at several pH values demonstrating different patterns of polyubiquitination preferences depending on the pH. **b)** Kinetic profiles, **c)** initial rates and maximum end-time FP values forming a bell-shaped distribution depending on the pH. **d-g)** PRT1-mediated ubiquitination of F-ek-Flv dependent on the concentration of E2-conjugating enzyme (UBC8). **d)** Time dependence of ubiquitination at several E2 concentrations for the first 60 min at 5 nM PRT1, time scale: 5-60 min. **e)** Michaelis-Menten curve plotted using the initial rate from FP data suggest an E2-driven inhibition effect. **f)** The qualitative evaluation of ubiquitination was done using in-gel scanning fluorescence and **g)** kinetic profiles were obtained using FP measurements, similar conditions as in d) but with ten times higher concentration of PRT1, i.e. 50 nM.

Another remarkable observation of the ubiquitination pattern in the in-gel fluorescence image (using three different independent substrate protein purifications of F-eK-Flv-NBD) is that the tri-ubiquitinated form presents three distinct subspecies which eventually lead to a multitude of other species at higher level (**Supplementary Figure 1b**). This could be explained by the possible formation of various ubiquitinated isoforms of the substrate fusion protein generated by utilizing different lysine side chains as ubiquitination acceptor sites. These could be either within the sequence of eK (e.g. Lys15 and Lys17) or within Flv (e.g. Lys100 and Lys222 which seem structurally more favored according to the structural model, **Supplementary Figure 1a**). This is further supported by the fact that there is only one species of tri-ubiquitinated F-eΔK-Flv-NBD, where two ubiquitination acceptors sites within eK (Lys15 and Lys17) were replaced by Arg (**Supplementary Figure 1b**).

Fluorescently labeled substrate proteins unravel mechanism of PRT1-mediated ubiquitination

The combination of the proposed two fluorescence-based methods allowed fast and efficient *in vitro* investigation of the ubiquitination process via the E3 ligase PRT1 and the optimization of the reaction conditions. In terms of applications, the kinetic approach allows collecting data that can assist to easily set up high-throughput assays by checking diverse variables in short time, e.g. for screens of inhibitors and small molecules potentially facilitating or enhancing ubiquitination. In our example, this included testing of the enzymatic parameters of E2-E3 interactions and substrate specificities for PRT1. Similar approaches have used labeling with radionuclides or fluorescent dyes coupled to Ub.⁴⁷ The latter covalent modification of Ub with fluorescent moieties is often impractical since these groups can sterically hinder the E1-catalyzed activation and E2-dependent transthiolation

reactions.⁴⁸ This in turn can alter the rate-limiting step. The use of radioactive isotopes requires at least running an SDS-PAGE and gel-drying or western blotting followed by autoradiography for hours to days.

Influence of the pH on PRT1 function as E3 ubiquitin ligase

As a first approach utilizing the real-time assay in the context of substrate ubiquitination, we studied the role of changes in pH on the ubiquitination process mediated by PRT1. A classical end-time approach revealed the reaction optimum to be clearly above pH 7 but below pH 9 as indicated by the occurrence of polyubiquitinated species of the fluorescent substrate probe F-eK-Flv-NBD (**Figure 3a**). However, using our real-time FP protocol, we additionally acquired the kinetic profile of the PRT1-mediated ubiquitination process (**Figure 3b**) and the maximum reached polarization values of this reaction (**Figure 3c**). These correlated with the amount of polyubiquitinated species detected in the SDS-PAGE gel-based end-time experiment (**Figure 3a**) and the highest initial rate (**Figure 3c**) whereas the latter appears to be different from the reaction optimum according to the detected max. FP. We also had previously observed, that F-eΔK-Flv ubiquitination presented a faster initial rate but only half of the final FP (**Figure 2f**) and lower degrees of final ubiquitination (**Supplementary Figure 1c**). Both bell-shaped forms of the pH dependence for the highest initial reaction rate (pH 8.0) and the maximum substrate polyubiquitination rate (pH 7.5) indicate two competing processes that generate a local maximum (**Figure 3c**). In the light of recently discussed mechanisms of E3 ligase action⁴⁹ and the predicted two RING domains of PRT1,³ higher ubiquitination rates with increased pH can be due to deprotonation of the attacking lysine side chain of the E2 active site. This facilitates thioester

cleavage between E2 and Ub and thereby mediates Ub transfer to the substrate lysine(s), an effect similar to the influence of the acidic residues in close vicinity of the E2 active site, which also cause deprotonation of the lysine side chain of the incoming substrate.⁵⁰ This possibly explains the drastic increase in the initial rate of PRT1 substrate ubiquitination in the pH 6.8 to pH 8 range (**Figure 3c**). The competing processes leading to the decrease in ubiquitination at pH>8 could be destabilization of ionic and hydrogen bonds at alkaline pH simply interfering with protein-protein interaction or ATP hydrolysis affecting the Ub charging of the E2 by the E1. This could also explain the premature leveling of the kinetic curves in the FP measurements at pH>8 (**Figure 3b**) while in a longer reaction timescale, the maximum FP values would be expected to be the same at pH 6.8 to pH 7.5.

Interaction of E3 ligase PRT1 with E2-conjugating enzymes

A strong decrease of the ubiquitination rate mediated by PRT1 was observed at higher concentrations of the E2-conjugating enzyme UBC8 (>2 μ M) both via in-gel fluorescence (**Figure 3d**) and FP (**Figure 3e-g**). Based on the FP measurements using up to 2 μ M of UBC8, the K_M of substrate ubiquitination by PRT1 at different E2 concentrations was found to be in the submicromolar range, 0.08 ± 0.01 μ M, indicating a very tight binding of the E2 to PRT1 compared to other RING E3 ligases⁵¹ (**Figure 3e**). The apparent catalytic rate constant (k_{cat}) of the Ub transfer, i.e. the rate limiting step, was found to be 1.30 ± 0.07 s⁻¹, which suggests that PRT1 has a high turnover number due to a highly active catalytic center. Moreover, the distribution pattern of the ubiquitinated substrate species at the end of the reaction (**Figure 3f**) and the kinetic profiles of ubiquitination (**Figure 3g**) are different, depending on the used E2 concentration. This suggests that the E2 concentration does not

only influence the rate of the Ub transfer to the substrate but also the mechanism itself. Possible causes are the two separate and potentially distinctly favored chain initiation and elongation processes mentioned above. These could result in lowering the rate of the initiation step at higher E2 concentrations since both the kinetic profile and the formation of ubiquitinated species are affected and also the attacking lysines could be structurally differently favored. This is especially suggested by the variable occurrence of the distinct pattern of triubiquitinated substrate species (**Figure 3d,f**) as mentioned above and discussed in other systems as well.⁵¹

MATERIAL AND METHODS

Cloning and expression of recombinant proteins

Artificial N-end rule substrates

Escherichia coli flavodoxin (Flv, uniprot ID J7QH18) coding sequence was cloned directly from *E. coli* DNA BL21(DE3) and flanked by an N-terminal triple hemagglutinin (HAT) epitope sequence using the primers Flv_rvs (5'-TTATTTGAGTAAATTAATCCACGATCC-3') and Flv_eK_HAT(oh)_fwd (5'-CTGGTGCTGCAGATATCACTCTTATCAGCGG-3'). The X-eK sequences comprising codons for various N-terminal amino acids exposed after TEV cleavage of the expressed X-eK-Flv fusion protein were cloned from an eK:HAT template using the primers eK(X)_TEV(oh)_fwd (5'-GAGAATCTTTATTTTCAGxxx CACGGATCTGGAGCTTG-3' with xxx=GTT (for Phe), GGG (for Gly), GAG (for Arg), and GTT (for Leu)) and eK_HAT_flav(oh)_rvs (5'-CCGCTGATAAGAGTGATATCTGCAGCACCAG-3'). This sequence contains a TEV protease recognition sequence (ENLYFQ|X with X being the neo-N-terminal after cleavage, i.e. TEV P1' residue) at the N-terminal of the expressed X-eK-Flv fusion pro-

tein. In order to attach Gateway attB sites and fuse the PCR products, a PCR was performed using Flv_attB2(oh)_rvs (5'-GGGACCACTTTGTACAAGAAAGCTGGGTA TCATTATTTGAG-TAAATTAATCCACGATCC-3') and adapter_tev_fwd (5'-GGGGACAAGTTTG TACAAAAA-GCAGGCAGGCTTAGAAAACCTGTAT TTTCAGGGAATG-3'). All primer sequences are listed in **Supplementary Table 1**. An LR reaction into pVP16⁵² (kind gift from Russell L. Wrobel, University of Wisconsin-Madison) lead to the final construct that consists of an N-terminal 8xHis:MBP double affinity tag. The expression vector pVP16::8xHis:MBP:tev:eK:3xHA:Flv was transformed into *E. coli* BL21(DE3) and the fusion protein was expressed by 0.2 mM IPTG induction in LB medium for 16 h at 26°C. Cells were harvested via centrifugation (3,500 g, 4°C, 20 min), resuspended in Ni-buffer (50 mM sodium phosphate pH 8.0, 300 mM NaCl), treated with 1mg/mL lysozyme (Sigma) in the presence of PMSF (Santa Cruz Biotechnology, sc-3597) added to a final concentration of 1 mM followed by sonication (4 min 40 %, 6 min 60% intensity). The lysate was centrifuged (12,500 g, 30 min), the supernatant loaded onto a Ni-NTA agarose column (Qiagen) equilibrated with Ni-buffer, followed by Ni-buffer washing, then the protein was eluted with Ni-buffer containing 200 mM imidazole (Merck) and loaded onto amylose resin (NEB). After washing with amylose-buffer (25 mM sodium phosphate pH 7.8, 150 mM NaCl), the protein was eluted with amylose-buffer containing 10 mM maltose. For TEV digest, the fusion protein was incubated overnight at 4°C with 0.27 µg/µL self-made TEV protease, expressed from pRK793 (Addgene, plasmid 8827), in 50 mM phosphate pH 8.0, 0.5 mM EDTA, 1 mM DTT and loaded onto a Ni-agarose column (Qiagen) equilibrated with Ni-buffer. The flow-through containing the tag-free X-eK-Flv substrate was concentrated with an Amicon Ultra-15 (Merck Millipore).

PRT1 cloning, expression and purification

The coding sequence of *Arabidopsis* PRT1 was cloned according to gene annotations at TAIR (www.arabidopsis.org) from cDNA. The Sequence was flanked by an N-terminal TEV recognition sequence for facilitated downstream purification using the primers ss_prt1_tev (5'-GCTTAGAGAATCTTTATTTTCAGGGGATGGCCGAAACTATGAAAGATATTAC-3') and as_prt1_gw (5'-GGGTATCATTCTGTGCTTGATGACTCATTAG-3'). A second PCR using the primers adapter (5'-GGGGACAAGTTTGTACAAAAAAGCAGGCTTAGAGAATCTTTATTTTCAGGG-3') and prt1_pos2_as (5'-GGGGACCACTTTGTACAAGAAAGCTGGGTATCATTCTGTGCTTGATGA-3') was performed to amplify the construct to use it in a BP reaction for cloning into pDONR201 (Invitrogen) followed by an LR reaction into the vector pVP16.⁵² Recombination into this Gateway destination vector containing a 8xHis:MBP coding sequence 5' of the Gateway cassette leads to an N-terminal 8xHis:MBP double affinity tag.

The 8xHis:MBP:PRT1 isolation, cleavage and purification was done as described above for the X-eK-Flv but the Ni-buffer contained 10% glycerol and 0.1% Tween 20.

Chemical labeling

10 μ M of purified X-eK-Flv was incubated for 1 h at room temperature with 100 μ M of the synthesized thiol reactive fluorogenic labeling dye in 20 mM Tris-Cl pH 8.3, 1 mM EDTA and 1 mM tris(2-carboxy-ethyl)phosphine (TCEP, Thermo Scientific). The reaction was stopped with 1 mM cysteine hydrochloride, the unreactive dye removed using 10 kDa cut-off Amicon filters (Merck Millipore) by three successive washing steps, and the labeling efficiency evaluated by fluorescence intensity of the labeled dye (Tecan M1000) and total protein concentration using infra-red spectroscopy (Direct Detect, Merck Millipore).

Chemical synthesis

The detailed synthesis protocols of the labeling probe NBD-NH-PEG₂-NH-haloacetamide are described in **Supplementary Methods**. In brief, the following synthesis steps were accomplished: 1) *tert*-butyl {2-[2-(2-aminoethoxy)ethoxy]ethyl}carbamate (NH₂-PEG₂-NHBoc); 2) NBD-NH-PEG₂-NHBoc; 3) NBD-NH-PEG₂-NH₂ hydrochloride; 4) NBD-NH-PEG₂-NH-iodo-acetamide; 5) NBD-NH-PEG₂-NH-iodoacetamide; 6) NBD-NH-PEG₂-NH-chloroacetamide.

tert-butyl {2-[2-(2-aminoethoxy)ethoxy]ethyl}carbamate (NH₂-PEG₂-NHBoc)

To a solution of 2,2'-(ethylenedioxy)-bis(ethylamine) (50.00 mL, 33.83 mmol; 495.6 %) in dry dioxane (190 mL), di-*tert*-butyl dicarbonate (14.90 g, 68.27 mmol, 100 %) in dry dioxane (60 mL) was added slowly and the resulting mixture was stirred at 25 °C for 12 h. The reaction mixture was filtered, the solvent was removed under reduced pressure and the remaining residue was dissolved in distilled water (300 mL). The aqueous phase was extracted with dichloromethane (3 x 250 mL). Finally, the combined organic phases were dried (Na₂SO₄) and the solvent was removed under reduced pressure to yield *tert*-butyl {2-[2-(2-aminoethoxy)ethoxy]ethyl}carbamate (NH₂-PEG₂-NHBoc) as light yellow oil (16.09 g, 64.8 mmol, 94.9 %). ¹H NMR (400 MHz; CDCl₃) δ: 1.42 (br. s., 2H), 1.42 – 1.46 (m, 9H), 2.87 – 2.90 (m, 2H), 3.32 (m, 2H), 3.52 (m, , 2H), 3.55 (m, , 2H), 3.61 – 3.64 (m, 4H), 5.13 (br. s., 1H) ppm; ¹³C NMR (100 MHz, CDCl₃) δ: 28.4, 40.3, 41.8, 67.1, 70.2, 73.5, 79.2, 156.0 ppm; ESI-MS m/z: 248.7 [M + H]⁺, 497.4 [2M + Na⁺]⁺; HRMS (ESI) calculated for C₁₁H₂₅N₂O₄ 249.1809, found 249.1809.

NBD-NH-PEG₂-NHBoc

To a suspension of *tert*-butyl {2-[2-(2-aminoethoxy)ethoxy]ethyl}carbamate (1.50 g, 6.04 mmol, 100 %) and sodium bicarbonate (1.01 g, 12.08 mmol; 200 %) in acetonitrile (30 mL), 4-chloro-7-nitrobenzofurazan (NBD) (1.80 g, 9.06 mmol, 150 %) in acetonitrile (30 mL) was added slowly over a period of 2 h and the resulting mixture was stirred at 25 °C for 12 h. The reaction mixture was filtered, the solvent was removed under reduced pressure, and the remaining residue was subjected to chromatography (silica gel, methanol / ethyl acetate, 5 : 95) to yield NBD-NH-PEG₂-NHBoc as a brown solid (1.89 g, 4.58 mmol, 75.9 %). M.p.: 85 – 86 °C; *R*_F = 0.56 (methanol / ethyl acetate, 5 : 95); ¹H NMR (400 MHz; CDCl₃) δ [ppm]: 1.42 – 1.45 (m, 9H), 3.31 – 3.37 (m, 2H), 3.54 – 3.56 (m, 2H), 3.58 – 3.60 (m, 2H), 3.61 – 3.71 (m, 4 H), 3.87 (m, 2H), 5.02 (m, 1H), 6.20 (d, *J* = 8.6 Hz, 1H) , 6.88 (m, 1H), 8.49 (d, *J* = 8.6 Hz, 1H); ¹³C NMR (100 MHz; CDCl₃) δ [ppm]: 28.4, 43.6, 68.1, 70.2, 70.2, 70.4, 70.5, 77.2, 98.7, 136.3, 143.9, 144.0, 144.0, 144.3, 155.9; ESI-MS *m/z*: 410.5 [M – H]⁺, 434.2 [M + Na]⁺, 845.4 [2M + Na]⁺; HRMS (ESI) calculated for C₁₇H₂₅N₅O₇Na 434.1646, found 434.1647.

NBD-NH-PEG₂-NH₂ hydrochloride

To a solution of NBD-NH-PEG₂-NHBoc (2.08 g, 5.06 mmol, 100 %) in dry methanol (20 mL), trimethylsilyl chloride (2.70 mL, 21.27 mmol, 500 %) was added *via* syringe and the resulting mixture was stirred at 25 °C for 12 h. The solvent was removed under reduced pressure. The remaining residue was suspended in diethyl ether (15 mL), filtered and the solid was washed with several portions of diethyl ether, and the remaining solid

Mot et al.

Fluorescent N-end rule substrates

was dried under reduced pressure to yield NBD-NH-PEG₂-NH₂ hydrochloride as a brown solid (1.56 g, 5.01 mmol, 98.9 %). The crude product was used without further purification. M.p.: 192 – 193 °C; ¹H NMR (400 MHz; CD₃OD) δ [ppm]: 3.09 – 3.11 (m, 2H), 3.64 – 3.76 (m, 8H), 3.87 – 3.90 (m, 2 H), 6.19 (d, *J* = 8.4 Hz, 1H), 8.45 (d, *J* = 8.7 Hz, 1H); ¹³C NMR (100 MHz; CD₃OD) δ [ppm]: 41.5, 41.7, 70.1, 70.3, 70.8, 73.2, 98.8, 123.0, 136.5, 144.1, 144.4, 144.8; ESI-MS *m/z*: 310.5 [M – 2H]⁺, 312.3 [M]⁺; HRMS (ESI) calculated for C₁₂H₁₈N₅O₅ 312.1303, found 312.1303.

NBD-NH-PEG₂-NH-iodoacetamide

To a solution of NBD-NH-PEG₂-NH₂ hydrochloride (202.3 mg, 0.65 mmol; 100 %) and *N,N'*-diisopropylethylamine (134.3 μL, 0.77 mmol, 120 %) in dry acetonitril (4.0 mL), iodoacetic anhydride (401.0 mg, 1.13 mmol; 174 %) was added slowly and the resulting mixture was stirred at 25 °C for 12 h. The solvent was removed under reduced pressure and the remaining residue was subjected to chromatography (silica gel, methanol / ethyl acetate, 10 : 90) to yield NBD-NH-PEG₂-NH-iodoacetamide as a brown solid (151.1 mg, 0.32 mmol, 48.5 %). *R*_F = 0.45 (methanol / ethyl acetate, 10 : 90); ¹H NMR (400 MHz; CDCl₃) δ [ppm]: 3.50 – 3.54 (m, 2H), 3.62 – 3.65 (m, 2H), 3.69 – 3.71 (m, 8H), 3.73 – 3.76 (m, 2H), 6.21 (d, *J* = 8.7 Hz, 1H), 6.55 (br. s., 1H), 6.95 (br. s., 1H), 8.48 (d, *J* = 8.6 Hz, 1H); ¹³C NMR (100 MHz; CDCl₃) δ [ppm]: 0.56, 40.1, 43.6, 68.1, 69.4, 70.3, 70.5, 136.4, 143.9, 144.3, 167.1; ESI-MS *m/z*: 478.3 [M – H]⁺, 502.1 [M + Na]⁺ + 981.3 [2M + Na]⁺; HRMS (ESI (negative modulus)) calculated for C₁₄H₁₇N₅O₆I 478.0229, found 478.0222.

NBD-NH-PEG₂-NH-chloroacetamide

To a solution of NBD-NH-PEG₂-NH₂ hydrochloride (202.5 mg, 0.65 mmol; 100 %) and *N,N'*-diisopropylethylamine (134.3 µL, 0.77 mmol, 120 %) in dry acetonitril (4.0 mL), chloroacetic anhydride (221.7 mg, 1.30 mmol; 200 %) was added slowly and the resulting mixture was stirred at 25 °C for 12 h. The solvent was removed under reduced pressure and the remaining residue was subjected to chromatography (silica gel, methanol / ethyl acetate, 10 : 90) to yield NBD-NH-PEG₂-NH-chloroacetamid as a brown solid (150.5 mg, 0.39 mmol, 59.7 %). *R*_F = 0.46 (methanol / ethyl acetate, 10 : 90); ¹H NMR (400 MHz; CDCl₃) δ [ppm]: 3.54 – 3.58 (m, 2H), 3.64 – 3.75 (m, 8H), 3.87 – 3.90 (m, 2H), 4.06 (m, 2H), 6.20 (d, *J* = 8.7 Hz, 1H), 6.90 (br. s., 1H), 6.98 (br. s., 1H), 8.48 (d, *J* = 8.6 Hz, 1H); ¹³C NMR (100 MHz; CDCl₃) δ [ppm]: 30.51, 42.7, 43.6, 68.1, 69.5, 70.3, 70.5, 136.3, 143.9, 144.3, 166.0; ESI-MS *m/z*: 386.1 [M – H]⁺, 410.1 [M + Na]⁺; HRMS (ESI (negative modus)) calculated for C₁₄H₁₇N₅O₆Cl 386.0873, found 386.0863.

Ubiquitination assay and in-gel fluorescence detection

3.4 µM (calculated according to the unlabelled protein) of the X-eK-Flv fluorescently labeled substrate (X-eK-Flv-NBD) were solved in 25 mM Tris-Cl pH 7.4, 50 mM KCl, 5 mM MgCl₂, 0.7 mM DTT containing 16 µM Ubiquitin from bovine erythrocytes (Sigma-Aldrich, U6253). For ubiquitination, 2 mM of ATP (New England Biolabs), 40 nM of E1¹⁵, 0.31 µM of E2 (UBC8)¹⁵, and 5 nM of E3 (8xHis:MBP-tagged or untagged PRT1) were added to the previous mix in a final volume of 30 µL and incubated at 30°C for 1 h. The reaction was stopped by adding 5X reductive SDS-PAGE loading buffer and incubating for 10 min at 96 °C followed by SDS-PAGE. The gels were scanned using fluorescence detection on a Typhoon FLA 9500 biomolecular imager (GE Healthcare) with a blue excitation laser (473

Mot et al.

Fluorescent N-end rule substrates

nm) LD and an LBP emission filter (510LP), then blotted onto a cellulose membrane and detected with either mouse monoclonal anti-Ubiquitin antibody (Ub (P4D1), sc-8017, Santa Cruz Biotechnology, 1:5,000 dilution in blocking solution [150 mM NaCl, 10 mM Tris-Cl pH 8, 3% skim milk powder, 0.1% Tween 20]) or mouse monoclonal anti-HA epitope tag antibody (HA.11, clone 16B12: MMS-101R, Covance; 1:1,000 to 1:5,000, in blocking solution) and goat anti-mouse IgG-HRP (1858415, Pierce; 1:2,500 to 1:5,000 dilution in blocking solution). The acquired images of the gels (prior blotting) were analyzed using the Gel Analyser densitometric soft (Gel.Analyser.com). Thus, one may use the same gel for both in-gel fluorescence detection followed by blotting and immunodetection.

The same gels that were detected via fluorescence scanning were blotted and detected with ECL without further processing such as stripping. Thus, fluorescent detection can be combined with ECL in one simple workflow. For evaluation of pH dependence, 50 mM Tris-Cl was used as a buffering agent at pH 6.75, 7.0, 7.5, 8.0, 8.5 and 9.0.

Real-time ubiquitination assay using fluorescence polarization

For fluorescence polarization (FP), the reaction mixture (24 μ L) containing all the components except the ATP was incubated in a 384 well microplate (Corning, Cat. No. 3712 or 3764) at 30°C in a M1000 infinite plate reader (Tecan) until the temperature was stable (typically 4-5 min) and the reaction triggered by adding 6 μ L of 10 mM ATP preheated to 30°C. FP was monitored every 2 min at 562 nm while the excitation wavelength was set to 470 nm. The M1000 fluorescence polarization module was calibrated using 10 nM fluorescein in 10 mM NaOH at P = 20 mP.

Structure modeling of the artificial substrate

The amino acid sequence of the artificial F-eK-Flv substrate was submitted to the Protein Homology/Analogy Recognition Engine V 2.0⁵³ (Phyre², Structural Bioinformatics Group, Imperial College, London) in both normal and intensive modes. The bests selected templates were found to be PBD ID: 3EDC for the eK region and 2M6R for the Flv part) and the model was visualized using ViewerLite (Accelrys Inc.).

ACKNOWLEDGEMENTS

We thank Marco Trujillo for expression clones of His:UBC8 and His:UBA1, discussions and constant support in ubiquitination-related issues and Angela Schaks for synthesis of the chemical probe. This work was supported by a grant for setting up the junior research group of the *ScienceCampus Halle – Plant-based Bioeconomy* to N.D., by the grant WE 1467/13-1 of the German Research Foundation (Deutsche Forschungsgemeinschaft, DFG) to B.W. funding E.P., a grant of the Leibniz-DAAD Research Fellowship Programme by the Leibniz Association and the German Academic Exchange Service (DAAD) to A.C.M. and N.D., and Ph.D. fellowships of the Landesgraduiertenförderung Sachsen-Anhalt awarded to C.N. and F.F. Financial support came from the Leibniz Association, the state of Saxony Anhalt, the Deutsche Forschungsgemeinschaft (DFG) Graduate Training Center GRK1026 “*Conformational Transitions in Macromolecular Interactions*” at Halle, and the Leibniz Institute of Plant Biochemistry (IPB) at Halle, Germany. To complete work on this project, a Short Term Scientific Mission (STSM) of the European Cooperation in Science and Technology (COST, www.cost.eu) was granted to A.C.M. and N.D. by the COST Action BM1307 – “*European network to integrate research on intracellular proteolysis pathways in health and disease (PRO-*

Mot et al.

Fluorescent N-end rule substrates

576 *TEOSTASIS)*". This work was partially funded by the grant DI 1794/3-1 of the German Re-
577 search Foundation to N.D.

578

579 **AUTHOR CONTRIBUTIONS**

580 A.C.M. performed the ubiquitination reactions and related analysis. E.P. and B.W. designed
581 and synthesized the fluorescent probe, B.W. supervised the chemical synthesis, M.K. estab-
582 lished PRT1 ubiquitination reactions, C.N. cloned and purified PRT1, F.F. cloned the X-eK-
583 HAT fragment and performed site-directed mutagenesis. N.D. and A.C.M. designed the
584 study, wrote the manuscript and designed the figures. All authors read and approved the
585 final version of this manuscript.

586 **SUPPLEMENTARY INFORMATION**

587

588 **SUPPLEMENTARY FIGURES**

589 **Supplementary Figure 1. Modeled structure of the F-eK-Flv substrate and PRT1 N-**
590 **terminal specificity.**

591

592 **SUPPLEMENTARY TABLES**

593 **Supplementary Table 1. Oligonucleotides used in this study.**

594

595 **SUPPLEMENTARY METHODS**

596 **Synthesis of the chemical probe NBD-NH-PEG₂-NH-haloacetamide.**

REFERENCES

1. Bachmair A, Becker F, Schell J. Use of a reporter transgene to generate arabidopsis mutants in ubiquitin-dependent protein degradation. *Proc Natl Acad Sci U S A* **90**, 418-421 (1993).
2. Potuschak T, Stary S, Schlogelhofer P, Becker F, Nejinskaia V, Bachmair A. PRT1 of Arabidopsis thaliana encodes a component of the plant N-end rule pathway. *Proc Natl Acad Sci U S A* **95**, 7904-7908 (1998).
3. Stary S, Yin X, Potuschak T, Schlogelhofer P, Nizhynska V, Bachmair A. PRT1 of Arabidopsis is a ubiquitin protein ligase of the plant N-end rule pathway with specificity for aromatic amino-terminal residues. *Plant Physiol* **133**, 1360-1366 (2003).
4. Bachmair A, Finley D, Varshavsky A. In vivo half-life of a protein is a function of its amino-terminal residue. *Science* **234**, 179-186 (1986).
5. Varshavsky A. The N-end rule pathway and regulation by proteolysis. *Protein Sci* **20**, 1298-1345 (2011).
6. Dougan D, Truscott K, Zeth K. The bacterial N-end rule pathway: expect the unexpected. *Mol Microbiol* **76**, 545-558 (2010).
7. Tasaki T, Sriram S, Park K, Kwon Y. The N-end rule pathway. *Annu Rev Biochem* **81**, 261-289 (2012).
8. Gibbs DJ. Emerging Functions for N-Terminal Protein Acetylation in Plants. *Trends Plant Sci* **20**, 599-601 (2015).
9. Gibbs DJ, Bacardit J, Bachmair A, Holdsworth MJ. The eukaryotic N-end rule pathway: conserved mechanisms and diverse functions. *Trends Cell Biol* **24**, 603-611 (2014).
10. Zenker M, et al. Deficiency of UBR1, a ubiquitin ligase of the N-end rule pathway, causes pancreatic dysfunction, malformations and mental retardation (Johanson-Blizzard syndrome). *Nat Genet* **37**, 1345-1350 (2005).
11. Piatkov K, Brower C, Varshavsky A. The N-end rule pathway counteracts cell death by destroying proapoptotic protein fragments. *Proc Natl Acad Sci U S A* **109**, E1839-1847 (2012).
12. Brower C, Piatkov K, Varshavsky A. Neurodegeneration-associated protein fragments as short-lived substrates of the N-end rule pathway. *Mol Cell* **50**, 161-171 (2013).
13. Shemorry A, Hwang C, Varshavsky A. Control of protein quality and stoichiometries by N-terminal acetylation and the N-end rule pathway. *Mol Cell* **50**, 540-551 (2013).
14. Kim H, Kim R, Oh J, Cho H, Varshavsky A, Hwang C. The N-Terminal Methionine of Cellular Proteins as a Degradation Signal. *Cell* **156**, 158-169 (2014).

15. Gibbs DJ, *et al.* Homeostatic response to hypoxia is regulated by the N-end rule pathway in plants. *Nature* **479**, 415-418 (2011).
16. Licausi F, *et al.* Oxygen sensing in plants is mediated by an N-end rule pathway for protein destabilization. *Nature* **479**, 419-422 (2011).
17. Gibbs D, *et al.* Nitric Oxide Sensing in Plants Is Mediated by Proteolytic Control of Group VII ERF Transcription Factors. *Mol Cell* **53**, 369-379 (2014).
18. Weits D, *et al.* Plant cysteine oxidases control the oxygen-dependent branch of the N-end-rule pathway. *Nat Commun* **5**, 3425 (2014).
19. Mendiondo GM, *et al.* Enhanced waterlogging tolerance in barley by manipulation of expression of the N-end rule pathway E3 ligase PROTEOLYSIS6. *Plant Biotechnol J* **14**, 40-50 (2016).
20. de Marchi R, *et al.* The N-end rule pathway regulates pathogen responses in plants. *Sci Rep* **6**, 26020 (2016).
21. Holman T, *et al.* The N-end rule pathway promotes seed germination and establishment through removal of ABA sensitivity in Arabidopsis. *Proc Natl Acad Sci U S A* **106**, 4549-4554 (2009).
22. Abbas M, *et al.* Oxygen sensing coordinates photomorphogenesis to facilitate seedling survival. *Curr Biol* **25**, 1483-1488 (2015).
23. Gibbs DJ, Conde JV, Berckhan S, Prasad G, Mendiondo GM, Holdsworth MJ. Group VII Ethylene Response Factors Coordinate Oxygen and Nitric Oxide Signal Transduction and Stress Responses in Plants. *Plant Physiol* **169**, 23-31 (2015).
24. Graciet E, *et al.* The N-end rule pathway controls multiple functions during Arabidopsis shoot and leaf development. *Proc Natl Acad Sci U S A* **106**, 13618-13623 (2009).
25. Yoshida S, Ito M, Callis J, Nishida I, Watanabe A. A delayed leaf senescence mutant is defective in arginyl-tRNA:protein arginyltransferase, a component of the N-end rule pathway in Arabidopsis. *Plant J* **32**, 129-137 (2002).
26. Schuessele C, *et al.* Spatio-temporal patterning of arginyl-tRNA protein transferase (ATE) contributes to gametophytic development in a moss. *New Phytol* **209**, 1014-1027 (2016).
27. Hoernstein SN, *et al.* Identification of targets and interaction partners of arginyl-tRNA protein transferase in the moss *Physcomitrella patens*. *Mol Cell Proteomics*, (2016).
28. Faden F, *et al.* Phenotypes on demand via switchable target protein function in multicellular organisms. *Nat Commun* **in press**, (accepted pending minor revision).
29. Sriram S, Kim B, Kwon Y. The N-end rule pathway: emerging functions and molecular principles of substrate recognition. *Nat Rev Mol Cell Biol* **12**, 735-747 (2011).

30. Venne AS, Solari FA, Faden F, Paretti T, Dissmeyer N, Zahedi RP. An improved workflow for quantitative N-terminal charge-based fractional diagonal chromatography (ChaFRADIC) to study proteolytic events in Arabidopsis thaliana. *Proteomics* **15**, 2458-2469 (2015).
31. Tsiatsiani L, *et al.* The Arabidopsis metacaspase9 degradome. *Plant Cell* **25**, 2831-2847 (2013).
32. Humbard M, Surkov S, De Donatis G, Jenkins L, Maurizi M. The N-degradome of escherichia coli: limited proteolysis in vivo generates a large pool of proteins bearing N-degrons. *J Biol Chem* **288**, 28913-28924 (2013).
33. Apel W, Schulze W, Bock R. Identification of protein stability determinants in chloroplasts. *Plant J* **63**, 636-650 (2010).
34. Garzón M, *et al.* PRT6/At5g02310 encodes an Arabidopsis ubiquitin ligase of the N-end rule pathway with arginine specificity and is not the CER3 locus. *FEBS Lett* **581**, 3189-3196 (2007).
35. Kumar E, Charvet C, Lokesh G, Natarajan A. High-throughput fluorescence polarization assay to identify inhibitors of Cbl(TKB)-protein tyrosine kinase interactions. *Anal Biochem* **411**, 254-260 (2011).
36. Smith M, *et al.* The E3 ubiquitin ligase CHIP and the molecular chaperone Hsc70 form a dynamic, tethered complex. *Biochemistry* **52**, 5354-5364 (2013).
37. Xia Z, Webster A, Du F, Piatkov K, Ghislain M, Varshavsky A. Substrate-binding sites of UBR1, the ubiquitin ligase of the N-end rule pathway. *J Biol Chem* **283**, 24011-24028 (2008).
38. Kapust R, Tozser J, Copeland T, Waugh D. The P1' specificity of tobacco etch virus protease. *Biochem Biophys Res Commun* **294**, 949-955 (2002).
39. Phan J, *et al.* Structural basis for the substrate specificity of tobacco etch virus protease. *J Biol Chem* **277**, 50564-50572 (2002).
40. Naumann C, Mot A, Dissmeyer N. Generation of artificial N-end rule substrate proteins in vivo and in vitro. *Methods Mol Biol*, (in press).
41. Stegmann M, *et al.* The ubiquitin ligase PUB22 targets a subunit of the exocyst complex required for PAMP-triggered responses in Arabidopsis. *Plant Cell* **24**, 4703-4716 (2012).
42. Sadowski M, Sarcevic B. Mechanisms of mono- and poly-ubiquitination: Ubiquitination specificity depends on compatibility between the E2 catalytic core and amino acid residues proximal to the lysine. *Cell Div* **5**, 19 (2010).
43. Lu Y, Wang W, Kirschner MW. Specificity of the anaphase-promoting complex: a single-molecule study. *Science* **348**, 1248737 (2015).
44. Petroski MD, Deshaies RJ. Mechanism of lysine 48-linked ubiquitin-chain synthesis by the cullin-RING ubiquitin-ligase complex SCF-Cdc34. *Cell* **123**, 1107-1120 (2005).

45. Deshaies RJ, Joazeiro CA. RING domain E3 ubiquitin ligases. *Annu Rev Biochem* **78**, 399-434 (2009).
46. Bachmair A, Varshavsky A. The degradation signal in a short-lived protein. *Cell* **56**, 1019-1032 (1989).
47. Melvin A, Woss G, Park J, Dumberger L, Waters M, Allbritton N. A comparative analysis of the ubiquitination kinetics of multiple degrons to identify an ideal targeting sequence for a proteasome reporter. *PLoS One* **8**, e78082 (2013).
48. Ronchi VP, Haas AL. Measuring rates of ubiquitin chain formation as a functional readout of ligase activity. *Methods Mol Biol* **832**, 197-218 (2012).
49. Berndsen CE, Wolberger C. New insights into ubiquitin E3 ligase mechanism. *Nat Struct Mol Biol* **21**, 301-307 (2014).
50. Plechanovova A, Jaffray EG, Tatham MH, Naismith JH, Hay RT. Structure of a RING E3 ligase and ubiquitin-loaded E2 primed for catalysis. *Nature* **489**, 115-120 (2012).
51. Ye Y, Rape M. Building ubiquitin chains: E2 enzymes at work. *Nat Rev Mol Cell Biol* **10**, 755-764 (2009).
52. Thao S, *et al.* Results from high-throughput DNA cloning of Arabidopsis thaliana target genes using site-specific recombination. *J Struct Funct Genomics* **5**, 267-276 (2004).
53. Kelley LA, Mezulis S, Yates CM, Wass MN, Sternberg MJ. The Phyre2 web portal for protein modeling, prediction and analysis. *Nat Protoc* **10**, 845-858 (2015).